**Research Article**          **Open Access**

# Multicellular Consortia Preserved in Biogenic Ductile-Plastic Nodules of Okondja Basin (Gabon) by 2.1 Ga

**Moussavou M[1], Edou-Minko A[1]\*, Mbina Mounguengui M[1], Ortega R[2,3], Fleury G[4], Roudeau S[2,3], Carmona A[2,3], Genty D[5], Blamart D[5], Tchikoundzi C[1], Makaya Mvoubou[1], Musavu Moussavou B[1], Ndong Ondo S[1], Ogandaga Agondjo M[1], Dewilde F[5], Delorme G[6], de Parseval Ph[7], Weil R[8] and Maire R[9]\***

[1]Universite des Sciences et Techniques de Masuku, BP:901 Franceville, Gabon, Africa
[2]Centre d'Etudes Nucléaires de Bordeaux Gradignan, Université de Bordeaux, Chemin du Solarium, F-33170 Gradignan, France
[3]Centre National de la Recherche Scientifique, IN2P3, CENBG, UMR5797, Chemin du Solarium, F-33170 Gradignan, France
[4]Muséum d'Histoire Naturelle de Toulouse, 35 Allée Jules Guesde, 3100 Toulouse, France
[5]Laboratoire des Sciences du Climat et de l'Environnement (LSCE), UMR 8212 (CEA/CNRS/UVSQ), L'Orme des Merisiers, 91191 Gif-sur-Yvette Cedex, France
[6]Geologue retraité de Comilog, Margnol, 24260 Mauzens-et-Miremont, France
[7]Geosciences Environnement Toulouse (GET), Observatoire de Midi-Pyrénées Université de Toulouse, CNRS, IRD, 14 Avenue Edouard Belin, F-31400 Toulouse, France
[8]Laboratoire de Physique des Solides, UMR 8502, Université de Paris Sud 91 405 Orsay cedex, France
[9]UMR 5185 ADESS, Maison des Suds, CNRS-Université Bordeaux-Montaigne-12, Esplanade des Antilles, Domaine Universitaire 33607 Pessac cedex, France

## Abstract

We highlight complex ductile nodules found in the $FB_2$ formation of the Okondja francevillian Basin (Gabon) dated to 2.1 Ga, during the Great Oxygenation Event (GOE). More than 500 specimens were collected from unmetamorphosed pelites in an excellent state of preservation. These nodules are divided into two groups: globular and elongated forms, one to three cm in diameter and over six cm long along the axis of elongation. They are characterized by two hemispheres separated by a central zone. They have a remarkable radial structure in spheroidal forms, and often have a polyphased structure in elongated forms. Chemical and microscopic analyses indicate that these nodules are formed over 80% of a fabric of micro-quartz, fossilizing calcite grains (rounded grains and remnants of biofilms) and clay channels. These slightly pyritized nodules also contain iron in the form of hematite and goethite.

There are several types of micro-organisms, several biomorphic iron particles (generally less than 300 µm in size) among which are preserved some multicellular clusters measuring between 50 and 250 microns, and some larger biomorphs. Their organization is very complex with fibro-radial and polyphased internal fabric and a discrete external peripheral system. The very low values of $\delta^{13}C$ carb in calcite (-17 and -26‰) suggest precipitation of calcite from decomposition of organic matter in anoxic photosynthesis conditions.

The morphological, petrographic, geochemical and isotopic characteristics of these nodules indicate a biological origin such as microbial/algal consortia, associated with eukaryotic organisms. They lived on the seafloor, buried just below the surface of the sediment, in calm, shallow and oxido-reducing environment.

## Introduction

The first period of net oxygen production in the Earth's history, referred to as the 'Great Oxidation Event' or 'GOE' [1-3], spanned c. 2.45 and 2.05 Ga [4,5], and is reflected in marine sedimentary rocks with extreme $\delta^{13}C$ ratios [1,6], increased seawater sulphate [7-9] and phosphate [10,11], and changes in iron redox speciation [12]. Although oxygen-producing cyanobacteria may have evolved earlier [13], they are widely believed to have contributed to the GOE, either directly [14] or indirectly [15]. Palaeobiological evidence for enhanced aerobic metabolism in this interval has, however, remained localised [16] and uncertain [11]. The c. 2.0-2.2 Ga Francevillian Group in the Republic of Gabon (Figures 1 and 2) has provided insights into the GOE in recent years, including redox indicators [12], Gunflint-type assemblages with purported cyanobacteria [17,18], and flattened pyrite nodules interpreted as large colonial aerobic organisms [19,20]. Eukaryotic algae have also been observed [21] or suggested locally by the presence of diverse and abundant steranes [22].

The Francevillian Group sediments and volcanic outcrop much of Gabon in four intra-cratonic basins formed during the extension of the Congo Craton (Figure 2) [23]. The Group is divided into five relatively unmetamorphosed lithostratigraphic units (FA-FE; maximum lower greenschist facies) and can be correlated across basins. Unit FA (<1.2 km) comprises fluviodeltaic and tidal deposits, including sulphates

[8,24]. Deep-water marine sediments at the base of the FB (<1000 m) reflect rifting and deepening. These include bituminous (<15% C) and phosphatic black shale, ironstone and Mn deposits [25]. In both the Franceville and Okondja basins, the lowermost FB (subunit $FB_1$) contains organic-rich black shale with intercalated Mn carbonate and iron oxide, primarily deposited under oxic conditions below the storm wave base [12]. Subunit $FB_2$ comprises alternating layers of quartz sandstone and black shale, and has recently been interpreted as part of a regressive sequence approaching the fair-weather wave base, whilst thin siltstones indicate waning storm surges [12]. In the Okondja basin,
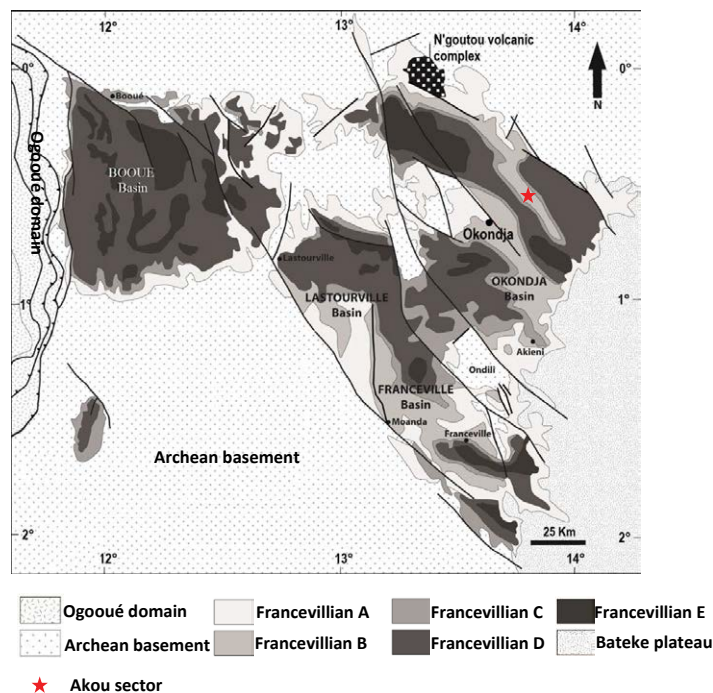
**Figure 1:** Geological map showing the context of fossiliferous Palaeoproterozoic rocks in Gabon. Archean basement is overlain by four sedimentary basins, including the Okondja Basin which contains the Akou nodules reported here modified from [23].
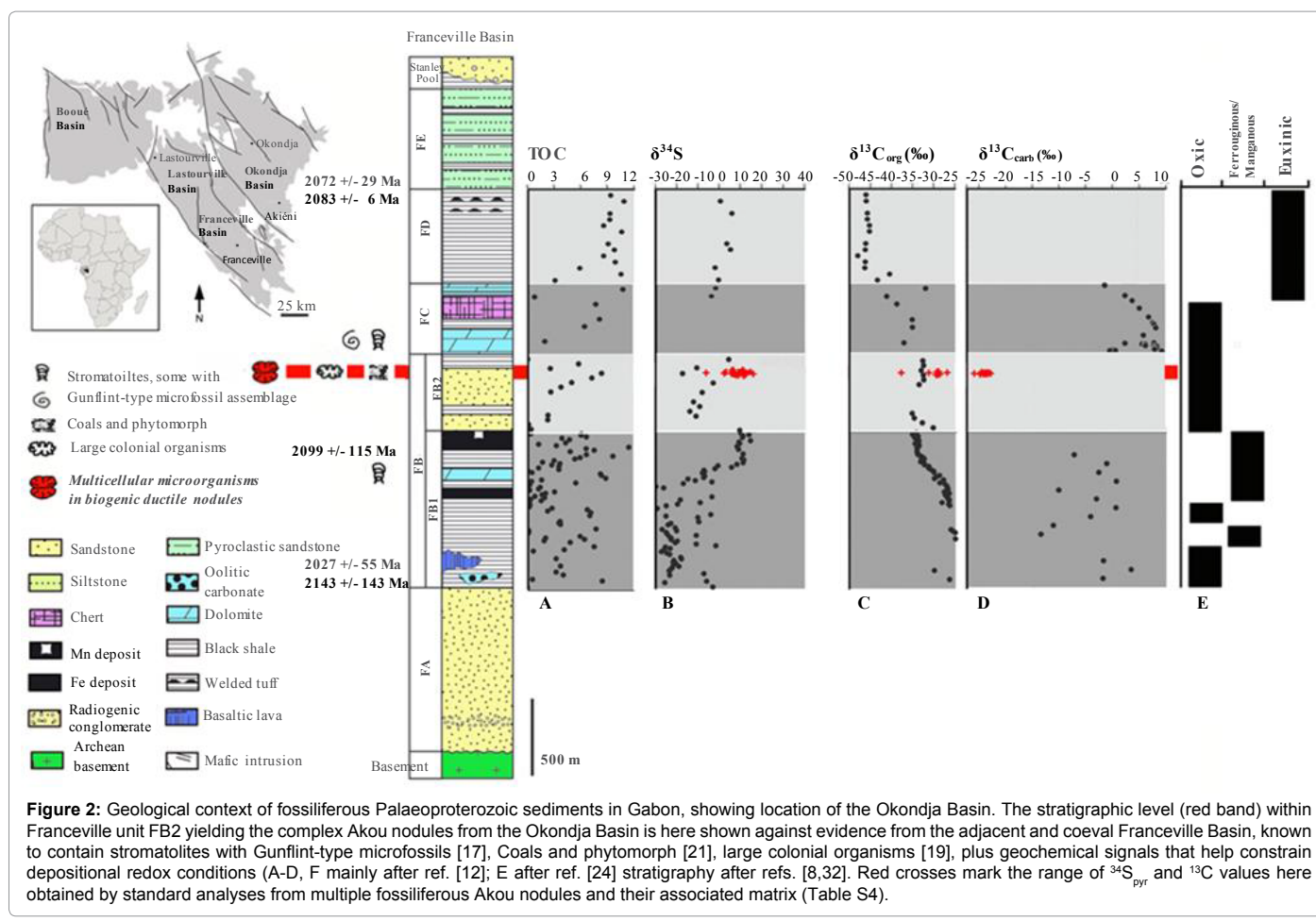


**Figure 2:** Geological context of fossiliferous Palaeoproterozoic sediments in Gabon, showing location of the Okondja Basin. The stratigraphic level (red band) within Franceville unit FB2 yielding the complex Akou nodules from the Okondja Basin is here shown against evidence from the adjacent and coeval Franceville Basin, known to contain stromatolites with Gunflint-type microfossils [17], Coals and phytomorph [21], large colonial organisms [19], plus geochemical signals that help constrain depositional redox conditions (A-D, F mainly after ref. [12]; E after ref. [24] stratigraphy after refs. [8,32]. Red crosses mark the range of $^{34}S_{pyr}$ and $^{13}C$ values here obtained by standard analyses from multiple fossiliferous Akou nodules and their associated matrix (Table S4).

subunit $FB_2$ shows alternations of sandstone and mudstone plus basic volcanics (Figure 3) [25].

All basin margins show shallower water conditions during FB times, with dolomite, sulphate evaporites and 'cyanobacterial' mats [8]. The FC unit is a thin (5-50 m) package of layered chert, jaspilite and dolomite, including silicified stromatolites with microfossils [18], likely formed under tidal and evaporitic conditions [8]. FD returns to deeper water conditions following tectonic rejuvenation, with 50-200 m of pyroclastic-bearing black shales [24]. Unit FE (c. 500-700 m), consists of alternating mudstones and sandstones rich in volcanic detritus [24,26].

The complex nodules are found near the top of sub-unit $FB_2$ within the Okondja Basin (Figures 1 and 2). Their age is constrained by diagenetic illites at the top of $FB_1$ (Sm-Nd age: 2099 ± 114 Ma) [12,26] and tuffs within FD (U/Pb age: 2083 ± 6 Ma [8,27] and 2072 ± 29 Ma [8,28]. Our material is therefore considered contemporaneous with large pyrite concretions from the Franceville basin (Figure 2) previously interpreted as mineralized organisms [19,20].

However, the Okondja nodules are slightly pyritous, frequently very flattened. These include crushed contact surfaces, dimples, lateral compression and internal furrows and channels (Figures 3e, 4g, 6j, 7, 8b, 10a, 11a2 and 11b1). Their occurrence is relatively widespread as they are also found in the Ngoutou region more than 50 km from the Akou River section.

## Data and methods

More than five hundred nodules and fragments were sampled in the Akou area. Hundred and ten nodules have been described and measured. Six powder samples including four nodules and two matrix sediments were analyzed by X-ray and over thirty nodules were observed under an optical microscope on thin and polished sections. Five nodules or fragments were observed by SEM. Four sedimentary plates containing nodules and fifteen nodules were analyzed at CT. Three nodules and one matrix sediment were analyzed at the nuclear microprobe using PIXE. Analysis of C, O, S stable isotopes were performed on thirty-two nodules and twelve matrix sediments.

The main analytical techniques are described:

**Lab-based CT analysis:** For groups of sediment-enclosed nodules, data were acquired using a General Electric LightSpeed CT scanner, with 0.5 mm slice thickness. For single nodules and specific areas from the above data were acquired on a Carl Zeiss Nanotom and a Carl Zeiss Metrotom, with slice thicknesses varying between 17 μm and 70 μm, depending on the size of the selected areas and Nanotom versus Metrotom CT equipment. All CT and microCT datasets were exported using the DICOM export file format to ensure best image quality and inter-operability. 2D and 3D imagery from CT and micro CT DICOM stacks were performed on a Dell Precision T7400 Dual Quad Core Intel Xeon 3.2 GHz using 32 GB of DDR RAM and a Quadro FX 4600 Graphics board running VG Studio Max 2.0 and 2.2 x 64 from Volume Graphics GmbH.

**PIXE analysis:** Nuclear microprobe analysis using PIXE (Particle Induced X-ray Emission) enables quantitative imaging of chemical element distributions in miscellaneous type of materials, including complex geological samples. In addition, the combination of PIXE with RBS (Rutherford Backscattering Spectrometry) provides fully quantitative concentrations of the chemical elements expressed in
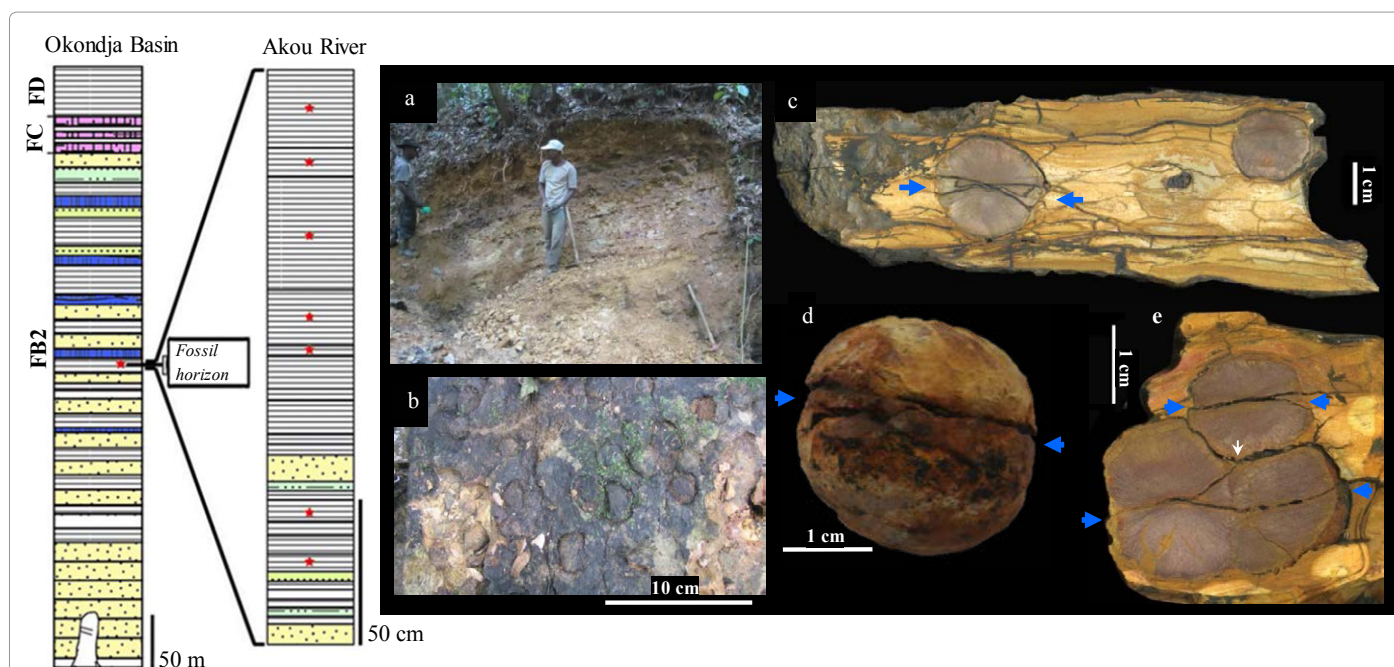


**Figure 3:** Lithostratigraphy of units FB2, FC and FD in the Okondja Basin, showing the location of complex nodules (red stars) in the Akou river section (key as for Figure 1) and the outcrop with the Akou nodules in the field; (A) Working face of the quarry near the Akou river that contains the fossiliferous nodules, showing beds of argillite, silt and thin sand sediment dipping gently to the left; (B) View of a bedding plane of the fossil level , showing a dense packing of subspherical to elongated nodules; (C) Vertical section though two adjacent subspherical nodules with median suture zones, showing compaction of sediment layers both below and above, consistent with their consolidation before or soon after burial by sediment (scan of the polished section); (D) Lateral view of a subspherical nodule, showing a median suture zone (blue arrows) separating an upper hemisphere from a lower hemisphere; (E) Vertical section showing the surimposition and interlocking of a subspherical nodule in an elongated nodule with a plastic deformation; the vertical stress (white arrow) shows that the "internal median surface" existed before the deformation. (scan of the polished section).

terms of gram of trace element per gram of sample, at the micrometer level. Thick sections of samples AKOU-14, AKOU-15 and AKOU-16 were analyzed using the PIXE microprobe at CENBG (Bordeaux-Gradignan). A proton beam energy of 1.775 MeV energy was chosen in order not only to give information on chemical elements distribution of Z>11 using PIXE, but also to enhance the carbon RBS signal through the carbon resonance at 1.75 MeV. The proton beam was focused down to the size of 2 micrometers onto the sample's surface reaching a beam intensity of 500 pA. The proton beam was raster scanned onto the sample allowing the chemical imaging of square regions of 1.2 x 1.2 mm². Chemical maps were recorded on 256 x 256 pixels matrix resulting in a spatial resolution of 4.6 µm /pixel. In the case of the AKOU16 fossil, 393 square zones of 1.2 x 1.2 mm² were analyzed to cover the full specimen section (about 576 mm²). Higher spatial resolution maps were also recorded on specific areas such as carbonate rich regions. In this case a smaller beam size (0.8 µm), with reduced beam intensity (180 pA), was scanned on regions of maximum 0.2 x 0.2 mm² area, with 256 x 256 pixels matrix, then reaching the highest spatial resolution of the setup (0.8 µm). Al, Si, S, K, Ca, Ti, Mn, and Fe distribution maps were obtained using PIXE analysis, while carbon and oxygen concentrations were determined simultaneously using RBS analysis. The quantification procedure was validated on U.S. Geological Survey Geochemical Reference Materials BCR2 (Basalt, Columbia River) and BIR1 (Icelandic basalt).

**Carbon, oxygen and soufre stable isotope analysis:** Stable oxygen, carbon and $\delta^{34}$S isotope ratios ($\delta^{18}$O, $\delta^{13}$C, $\delta^{34}$S), expressed in‰ VPDB (Vienna Pee Dee Belemnite standard) and in‰ VCDT (Viena Canyon Diablo Troilite standard), were performed at Laboratoire des Sciences du Climat et de l'Environnement on GV Isoprime mass-spectrometers and at Plateforme SF4206 ICORE (Interactions cellules, organismes, environnement) on EA 3000, EuroVector combined with a mass-spectrometer (Horizon, NU Instruments). $\delta^{13}C_{total}$ refers to analyses of samples prior to decarbonation, $\delta^{13}$Ccarb refers to analyses of calcite, $\delta^{13}$Corg referring to analyses after decarbonation.

**SEM analysis**: A scanning electron microscop (SEM) was used to perform observations and chemical analyses. It was a Zeiss supra55vp sem equiped with an energy-dispersive X-ray spectrometer (Bruker SDD detector) of Laboratoire de Physique des Solides de l'Université Paris-Sud 11. This field-effect "gun" microscope (FE-SEM) operates at 0.5-30 kV. High-resolution observations were obtained by 2 secondary electron detectors: an in-lens SE detector and an Everhart-Thornley SE detector. To maintain the integrity of the samples measurements were taken without the usual deposits of carbon or gold at the surface of the sample. Analysis complements were performed on JEOL 6360LV SEM and Bruker SDD XFLASH 5010 at GET of Toulouse.

# Results

## Akou nodules morphology

A succession of complex nodules are traceable through ~2 m of siliciclastic sediments, exposed in the Okondja Basin near the Akou River sections of unit $FB_2$ (Figure 3). These are ovate to elliptical (Figures 3-7, S1-S3, S6 and S7) and sharply delineated from the surrounding fine-grained uncleaved mudstone, and rippled silt and sand beds-sediments consistent with a quiet, non-hydrothermal, sedimentary regime stirred by occasional storms. Adjacent sediment layers are draped around nodules (Figure 3c and 4h), consistent with syn-sedimentary formation, pre-compactional, endobenthic nodule within shallow layers of sediment.

Nodules can be isolated (Figures 3c and 4h), grouped, often laterally paired (Figures 3e, 4g, 4h, 5j, 5k, 7a and 7b), aligned in curved chains (Figures 7c and 7d), or clustered (Figures 7e-7g) into groups in a bedding plane.

Individual nodules range in width from 0.7 cm to 6.2 cm, smaller examples tending to spheroidal, and larger ones ranging from spheroidal to ellipsoidal, wider than long (Figures 4, 5, S1 and Table S1).

Spheroidal nodules are often characterized by a tripartite structure with two hemispheres separated by a median zone (Figures 3c, 3d, 4a, 4b and S3). In some cases however, the median structure is lacking and the nodules have single globular form (Figure 4f). They are symmetrical
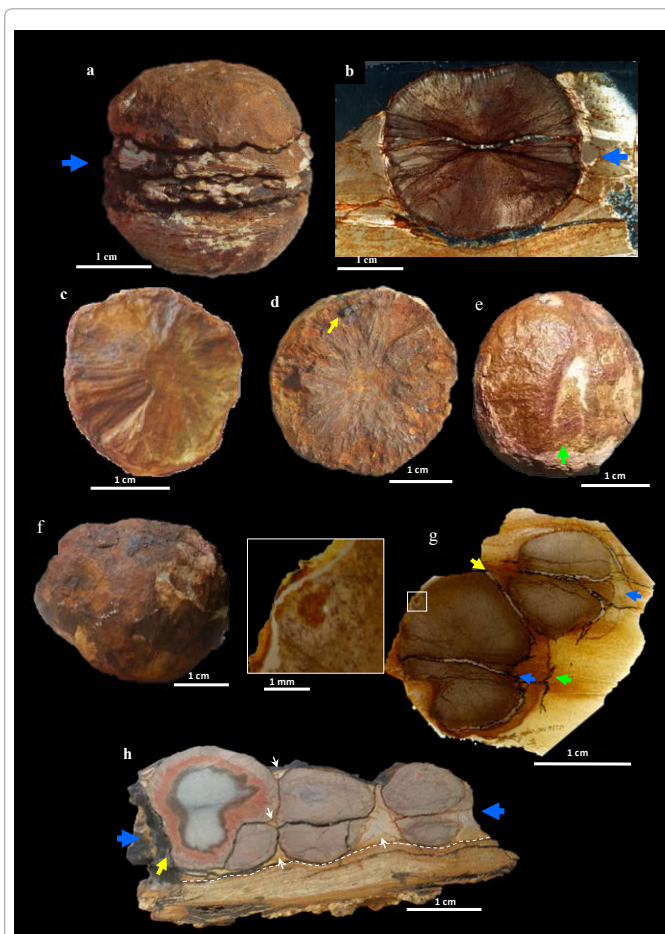


**Figure 4:** Spheroidal nodules. (A) Lateral view of a typical nodule, show a horizontal median zone with three cracks, separating an upper hemisphere from a lower hemisphere. (B) Vertical section showing the internal structure of a typical spheroidal nodule with tubular shapes well developed in the median zone (blue arrow); (C) Top view of a mediane zone, with a radial system very developed around the central cone; (D) Top view of a mediane zone, with a radial system developed around the central cone; and some ferruginous oblong shapes intersecting the radial system (yellow arrow); (E) Upper hemisphere of a nodule showing wide dimple on the top (green arrow); (F) View of a whole nodule; (G) Two contiguous spheroidal nodules, with a flat contact surface (yellow arrow) and the median zones displaced (blue arrows); showing also a translucent outer band follows the contour of the nodule (green arrow) and a raised border (sidebar), (OKO-012012); (H) View of a vertical section of three spheroidal nodules more or less weathered in sediment; two are adjoined with deformed contact surfaces and an isolated nodule, showing compacted sediment between them (white arrows); the yellow arrow shows a crushed contact surface; the blue arrows indicate the median zone; note the low ripple sediment below nodules (dotted lines).

along the vertical axis, have a complex internal radial fabric (CIR), (Figures 3c, 4b, S2c and S3).

The median zone is characterized by a biconcave or horizontal surface. It forms a "belt" that is 3 to 5 mm thick at the periphery of the nodule and gradually thins towards the centre to make way for a central zone of a few mm in diameter (Figures 3c, 4a, 4b, S2c and S3). It is made up of a multitude of filamentous shapes, arranged in very pronounced radial system around the central cone (Figures 4c, 4d, 7b and S2h). The internal median surfaces separate the median zone and hemispheres. This median zone is very vulnerable to weathering after fossilization and highly susceptible to cracking and degradation (Figures 4d, S3g and S3h). The median suture zone can also be fossilized and form a median 'disc' within the nodule (Figures 4a-4c, 7b and S3b-S3e).

The elongated specimens have several forms: ovoid, sausage, "double nodule"and segmented which can contain up to three contiguous segments (Figures 5 and 6). The common characteristics of these elongated shapes are:
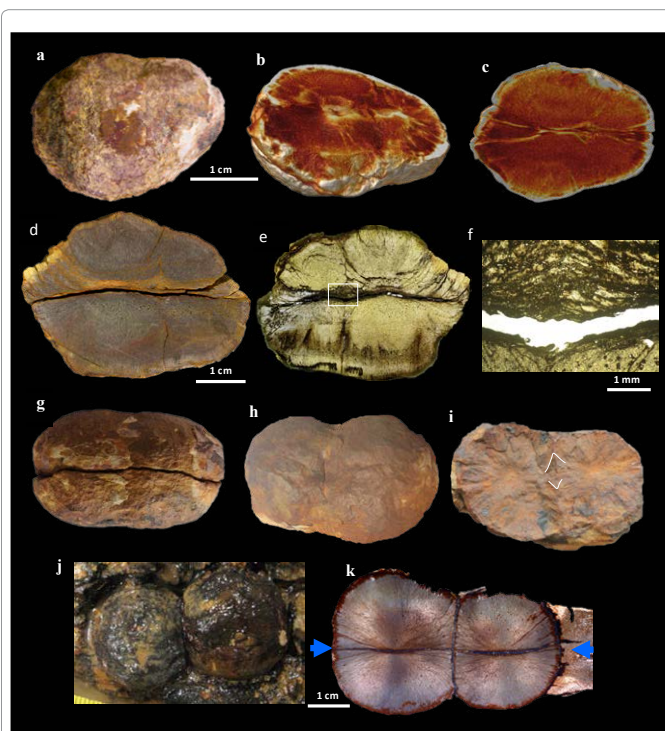


**Figure 5:** Various morphologies of elongated forms and "double nodule". (A-C) Ovoid form: (a) Macroscopic top view, (b) Same specimen showing in tomographic horizontal, a double internal radial system at the median zone, (c) Same specimen showing in tomographic vertical, an internal polygonal structure of both sides of the median surface; (D-F) Ferruginous elongated form: (d) Vertical polished section showing two hemispheres with curved median 'disc' and channels at the two ends, separated by a continuous median surface, (e) Scan of vertical thin section showing a polygonal structure at the centre, (f) Detail of the polygonal structure showing both sides of the internal median surface of the nested lenticular system above, and larger conical forms below; (G-I) Ferruginous elongated form: (g) Lateral view of an elongated nodule, show a horizontal median zone with a small strangulation of the two hemispheres perpendicular to the elongation of the nodule, (h) top view of upper hemisphere showing a strangulation perpendicular to the elongation of the nodule, (i) Horizontal unpolished median zone showing a double radial system linked by a linear suture of the polygonal structure (white '>'), joining the two edges and perpendicular to the elongation of the nodule; (J) Conjoined nodules with linear contact; (K) Vertical section through two conjoined specimens showing weathered margin, radial fabric, linear contact surface and continous median internal sutures (blue arrows indicate the median zone).
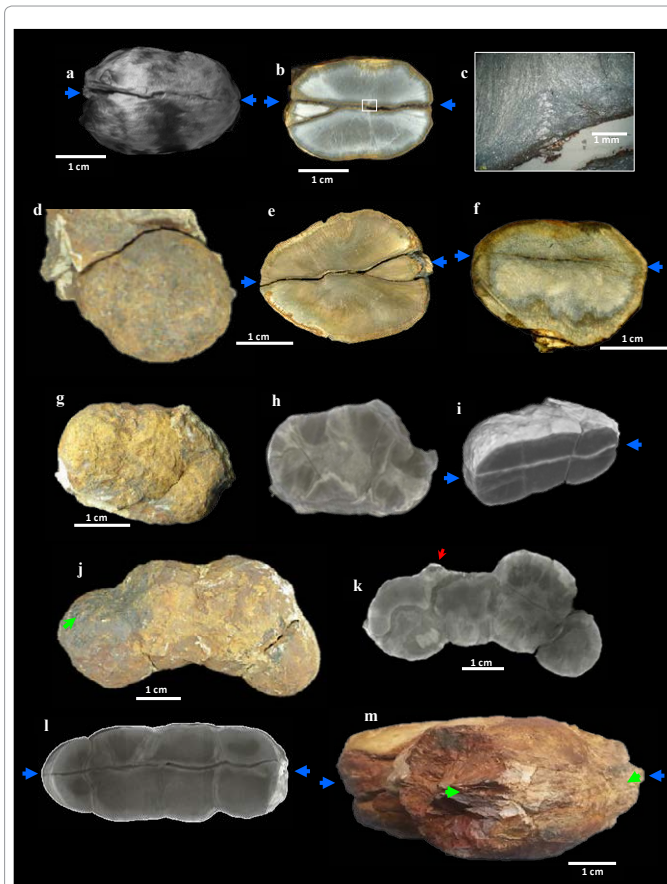


**Figure 6:** Various morphologies of elongated forms. (A-C) Elongated unsegmented silicified 'sausage' shape: (a) Specimen composed of two hemispheres separated by a median surface, (b) Polished section showing the extreme left-hand side of the median zone with a polygonal structure at the centre, (c) Detail of the polygonal structure; (D-E) Top view and vertical section of an ovoid nodule showing two hemispheres separated by a median surface, with a part of the "median disc" at the right end; (F) View of a polished section showing an elongated whole nodule with a flattened upper hemisphere, the internal median surface is barely visible (AKOU-16); (G-I) Three-segments specimen, (g) Macroscopic view showing barely visible segmentation, (h) Tomographic view showing three internal "median disc", (i) Tomographic view showing an internal median continuous surface on all segments; (J-L) Four-segments specimen, (j) A macroscopic view with a visible dimple on three segments (green arrow), (k) A horizontal tomographic view showing four internal "median disc" with "raised border" (red arrow); (l) A vertical tomographic view showing an internal median continuous surface on all segments and on the extreme right a part of the "median disc"; (M) Red ferruginized specimen showing a longitudinal furrow with a repeating pattern (green arrow). Blue arrows indicate the median zone.

a. A bipartite structure with two hemispheres separated by an internal median surface (Figures 5c-5e, 5g, 6a, 6b, 6e, 6f, 6i and 6l)

b. Sometimes a visible "strangulation" between segments (Figures 5g, 5h, 6j and 6l)

c. A polygonal internal structure, consisting of an area traversed by many criss-crossed by clayey channels, or with the crislallisation of calcite in a nested lenticular system non-radial (Figures 5c, 5e, 5f, 5i, 6b, 6c, 11a, 11a1 and 11b1)

d. A rectiligne suture into ovoid and "double nodule" shapes, or between two segments in the same elongated nodule; these

internal sutures, very slightly marked, are often straight and are not flattened (Figures 5i, 5k, 6i and 6l)

e.  In vertical section, the presence of a part of "median disc" at the extremities (Figures 5c, 5d, 6b, 6e and 6l)

f.  In horizontal section, the presence of "median disc" at each segment (Figures 5b, 5i, 6h, 6k and 7b)

Repetitive patterns in a rectilinear furrow are sometimes observed in the median zone of elongated nodules (Figure 6m). Elongated nodules are specific and do not seem to come from a fusion of spheroidal nodules that have 'grown' together

The deformations affect indifferently spheroidal shapes and elongated forms (Figures 3e, 4g, 4h, 6f, 6j and 7). They show evidence of crashes and plastic deformations on contact surfaces. The median zone, for example, can be without distortion (Figure 5k) or very distorted (Figures 7f and 7g) between two or three contiguous nodules. These deformations are generally lateral and are the result of compression with very little vertical elongation (Figure 7), compression can reduce the nodule by more than 50% of its theoretical volume (Figures 7c and 7g). The ductile body nodules are sometimes marked by external crushed contact surface, "dimple" and "raised border" (Figures 3e, 4e, 4g, 4h and 6k) and flattening internal clay channels (Figures 11a1 and 11b1). These deformations occurred in sedimentary beds that were very little deformed, with small ripples above and below nodules, and compacted sediment between them (Figures 3c and 4h).

The polyphased organization of nodules (complex internal radial, nested lenticular system, internal furrows, linear and flattened clay channels) suggests that these latter were formed in endobenthic conditions from an organized organic structure that probably existed before burial.

**Petrology, mineralogy and geochemistry**

Nodule and sediment mineralogy (Table S2, Figure S4d), and elemental geochemistry (Table S3, Figures S4a-S4e) were studied at the mm to nm scale. Four major components were identified: detrital silicate, secondary micro-quartz, calcite and pyrite (often altered to iron oxide). Detrital silicates (quartz, mica, clay and zircon) are conspicuous in the enclosing sediment. K-rich silicates are also concentrated in radiating channels within each nodule, some of which are connected to surrounding K-rich sediments (Figures 11a, 11b, 11b1, S6, S7a1, S7a2 and S7a4). In general, these clay channels have a radial position, but are often curved, sinuous or criss-crossed (Figures 11a2 and S7a4). PIXE chemical mapping (Fe/K/Ca) of AKOU-16 clearly illustrates this variability in channels and the peripheral clay "covering" (Figures S7a1 and S7a4). An example is the clay channels in AKOU-16 nodule, in the flattened zone of the upper hemisphere, highlighted by the K mapping (Figures 11b and 11b1). This flattening of clayey channels seems indicate the existence of an organized structure before burial.

Silica is the principal element of fossilization. The nodules largely consist of micro-porous and microcrystalline silica mass with average quartz grain size of 2 μm to 5 μm (Figures S5a and S5b). In addition, some macro quartz (>10 μm) is recrystallized in the voids and aligned in the same direction as the micro-quartz (Figures S5c and S5d). It is mainly microcrystalline quartz that has fossilized the fine radial structure of nodules (Figures S5a and S5b).

The microscopic observations and the chemical imaging (PIXE) show that calcite is pure and non ferroan (Figures 9f and 9g). Calcium carbonate show an amorphous structure, forming extended biofilm

(several tens of microns in size) or ranges interrupted grains with no clear direction (Figures 9a-9d). This 'calcite' biofilm recalls calcitic organominerals [29-31], as well as calcite influenced by secondary alteration and corrosion. In Akou-15 nodule, a remnant of calcitic biofilm 60 μm long show clearly a process of silicification with a transition phase between calcite and quartz (Figure 9e). A part of the crystallized calcite was detected by RX (Figure S4e).

Calcite forms an important part of the fabric of the nodule and it is uniformly distributed throughout the structure, and often in criss-crossed bands or furrows (Figures 8 and 10a). Most of the calcite grains (2-30 μm) are locally conjoined and form clusters of several tens of μm with a main radial direction and internal secondary direction (Figures 10a-10f). Calcite also features globular forms with bristly surfaces (Figures 10g and 10h). Like silica, these calcite clusters have preserved the fine texture of the nodule and sometimes show alignments in 'furrows' (200 μm wide) that are oblique to the main radial direction
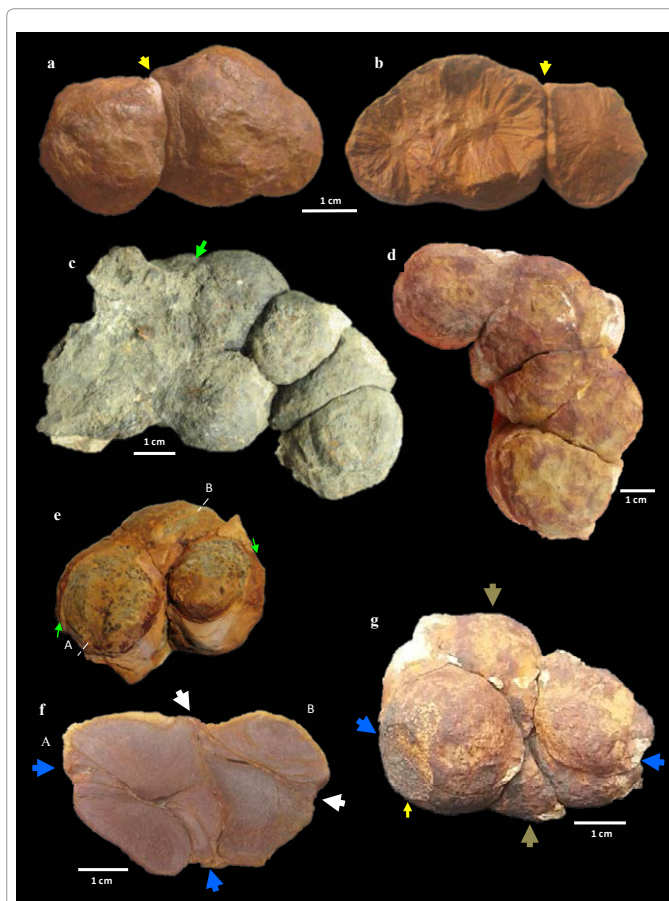


**Figure 7:** Deformation of nodules. (A-B) Top and internal views of a spheroidal nodule attached to an elongated nodule; the elongated nodule has a double internal radial system with flattened surfaces (yellow arrow) suggesting that the two types of nodule were formed differently; (C) View of five contiguous and highly laterally distorted nodules, with alignment in sediment (green arrows); (D) View of five other contiguous, laterally deformed nodules; (E-F) Three contiguous nodules, deformed by lateral compression and partially covered by a "thin ferruginous pellicule" (green arrows), (e) Full view of three contiguous nodules, (f) Vertical section of two nodules-showing a very deformed sinuous contact, with downwards movement of the median zone of one (blue arrow) and upwards movement of the other (white arrow); (G) Three other contiguous nodules deformed by lateral compression, the nodule to middle (grey arrows) shows two hemispheres strongly compressed at the median zone (blue arrows), (yellow arrow indicates a flattened contact surface.
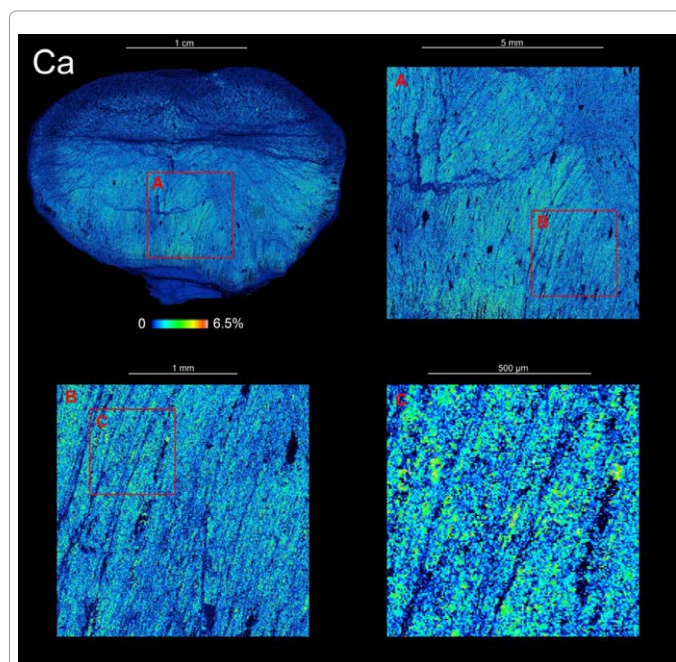
**Figure 8:** Micro-PIXE images of a vertical section through an elongated Akou nodule (AKOU 16). These confirm that Ca ion distribution is arranged in radial bands, related to the calcite sub-crystals. Progressive crystallization of calcite is shown of the highlighted central region showing the microgranular structure of the calcite, with numerous furrows more or less criss-crossed. The images are composed of 393 individual scans of 1.2 x 1.2 mm², recorded with a spatial resolution of 4 μm. The color scale is quantitative, with red pixels the maximum observed values for each element. Scale bars = 1 cm, 5 mm, 1 mm and 500 μm respectively.

(Figure 10a) or two different contiguous structures (Figures 10c and 10d). These observations suggest an early phase of calcite precipitation, which preserved the internal structure of the nodule in great detail. Levels of calcite $\delta^{13}C_{carb}$ values of -17 to -26‰ VPDB (mean-24‰; n=30 across 12 nodules; (Figure S8 and Table S4) show that nodules are significantly more $^{13}$C-depleted than bedded dolostones from the Lastourville Basin at Lastourville ($\delta^{13}C_{carb}$ 5 to 6‰; n=7; Figure S8 and Table S4). These are also more $^{13}$C depleted than broadly coeval bedded carbonates within the Lastourville and Franceville Basins, including the black shales and blocks of dolostone from FB, and dolostones in FC ($\delta^{13}C_{carb}$, -11.1‰ to 9.7‰) [8,32]. $\delta^{13}C_{org}$ values from within nodules and matrices range from -26 to -37 ‰(av. -29.43‰; n=11; Figure S8 and Table S4); these are close to $\delta^{13}C_{org}$ values reported from comparable levels in the Franceville Basin (Figure 2) [11]. Micro-PIXE analyses clearly reveal that most pyritic and iron oxide biomorphs are aligned with the radial axes (Figure 11a), although some cross-cut and/or have a sinuous shape. Bulk sulphur isotopes analyzed from pyrite grains within 21 nodules reveals $\delta^{34}S_{pyr}$ values ranging from -7 to 18‰ (Table S4), with most having values above 7‰. Around the nodule exteriors, pyrite has typically been altered to a rubified zone of iron oxide, including hematite and goethite (Figures 11a and S6). These pyrite-biomorphs correspond to pyritization of organic filaments and particules (Figures 14d and S9c) by sulphate-reducing bacterial activity.

A notable feature of AKOU-16 nodule is filaments and particles of iron oxides, which are more or less elongated and probably biomorphs. In the lower unflattened hemisphere these filaments, sometimes associated with clays, are linear and often discontinuous, while particles are scarce and largely concentrated at the edge. In the flattened upper hemisphere, iron particles predominate and are

above all aligned, generally in an upright position in the clay channels (Figures 11a, 11b, 11a1 and 11b1). AKOU-1 also contains a multitude iron particles aligned in the radial system; there is also the presence of a larger ferruginous filament intersecting the radial direction (Figure 12a). It is among these iron particles, it was described some pockets with translucent pellicular envelope containing spherulites (Figures 12a1 and 12b), and some spherulites whose color varies by type of fossilization (Figures12c-12f).

Other micrometric biomorphs are also common in nodules. They tend to be randomly distributed, and are often either aligned with radial internal structures, or intersect them.

The high positive values of $\delta^{13}C_{carb}$ from black shales, dolomites and stromatolites, depleted $\delta^{13}C_{carb}$ from early-formed calcite in the nodules, and depleted $\delta^{13}C_{org}$ in their organic matter and in the black shales, dolomites and stromatolites, suggest early calcite precipitation in a closed and reduced environment. Into the nodules, the calcite precipitation (biofilm) was triggered by an EPS recation of cyanobacteria [32-34].
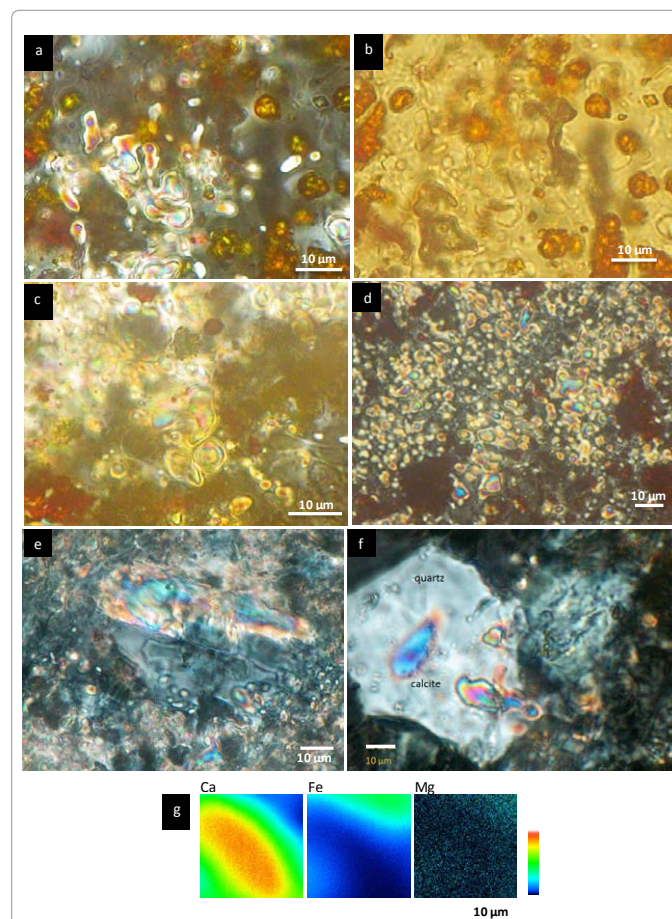


**Figure 9:** Elements of calcite biofilm in nodule; (A-B) Biofilm and amorphous calcite with ferruginous spherulites, (a, crossed nicols; b, parallel nicols, OKO-3b); (C) Calcite biofilm with hematite (crossed nicols , FRA-21); (D) Unjoined calcite grains which would come from the alteration of the calcite biofilm (crossed nicols, OKO 3b); (E) Area of biofilm and calcite grains with micro-quartz (chert) showing a transition between calcite biofilm and quartz (crossed nicols, AKOU-15); (F) Calcite grain analyzed PIXE is located in the secondary quartz; other calcite grains are located at different levels of quartz, (yellow arrow) (crossed nicols, AKOU 16); (G) PIXE element maps of a typical calcite micro-grain, showing Ca, Fe and Mg patterns consistent with non-ferroan calcite (AKOU 16). Scale bars :10 μm.
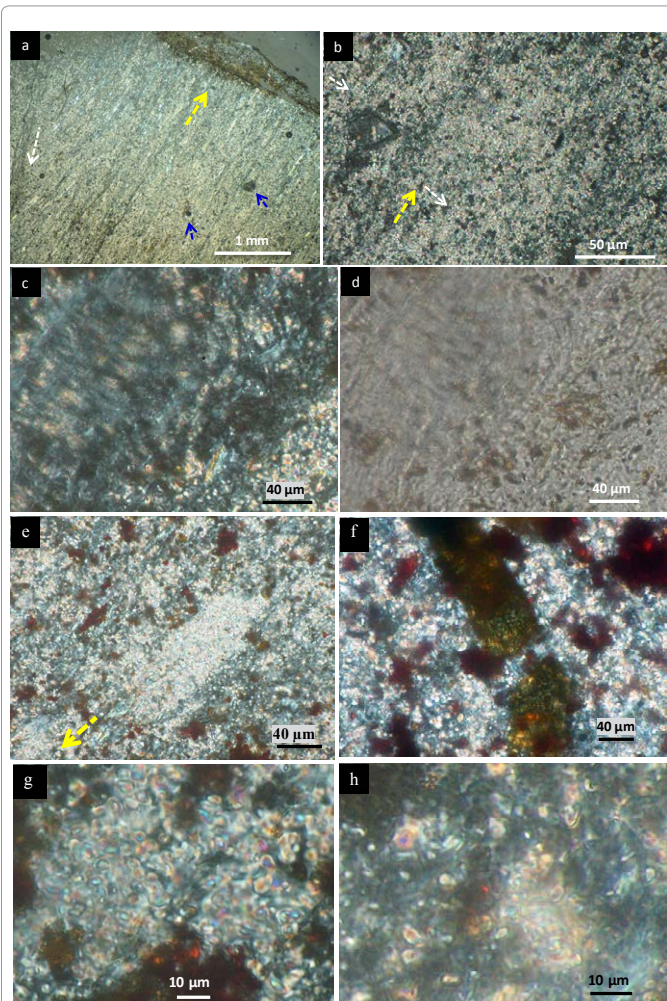
**Figure 10:** Calcitic structures in nodules using optical microscopy on thin sections (crossed nicols). (A) Almost continuous area of calcite micro-granules within a radiating calcite band (yellow arrow) marked by a secondary oblique groove (200 μm wide), iron particles that intersect the radial system (blue arrows); (B) Almost continuous area of calcite micro-granules running in two directions: a main radial direction and a secondary direction (AKOU-13). (C-D) Area of calcite showing micro-grains in curved alignment that intersects a grey area with broader, diffuse patches of calcite (crossed nicols and parallel nicols, AKOU-13). (E) Example of biofilm, the yellow arrow shows the alignment of a continuous area of calcite micro-grains (AKOU-13). (F) Area of calcite grains associated with a green algal band and strains of iron oxides running in the same direction (OKO-1). (G) Very dense calcite grains (3-5 μm in size), associated with ferruginous biomorphs. (AKOU-13). (H) Calcitic globular grains showing a bristled surface (AKOU-13).

$\delta^{34}S_{pyr}$ values match those expected from bacterial sulphate-reduction at this time [35]. The $\delta^{18}O$ values which correspond to those of Paleo-Proterozoic oceans are between -17 and -7‰, probably with a local alteration of the oxygen ion, without which the best estimate of $\delta^{18}O$ values of these oceans is between -11 and -7‰ [36].

The $\delta^{18}O$ values of FB sedimentary carbonates and FC stromatolites, from -12.70 to -5‰ [8], and those of oceans are in the same range. This suggests that oxygen of $CaCO_3$ sedimentary carbonates and stromatolites was in isotopic equilibrium with the seawater. By against, the $\delta^{18}O$ values of calcite in nodules, from -14 to -11.90‰ (Figure S8 and Table S4) are lower and indicate some alteration of the oxygen ion in anoxic conditions. Biogenic calcite of nodules therefore would come of

an extracellular biomineralization process linked to the microorganism action in a reducing environment.

Mineralogical and geochemical data clearly suggest a process linked to the decomposition of organic matter in the nodule under reduced and closed conditions favouring the formation of early (primary) biogenic pyrite, biogenic calcite; and relatively late primary silicification due to silica which was abundant in the Proterozoic oceans [37].

### Microorganisms and biomorphs

Various types of microorganisms and multiple biomorphs can be observed with optical microscopy and scanning electron microscopy (SEM). However care must be taken as morphological indicators are not always sufficient. For example, here we do not take into account filamentous textures generated by *Gallionella-* and *Leptothrix*-type bacteria that are related to the alteration of ferrous iron phyllosilicates in both nodules and the sediment matrix. However, other observations
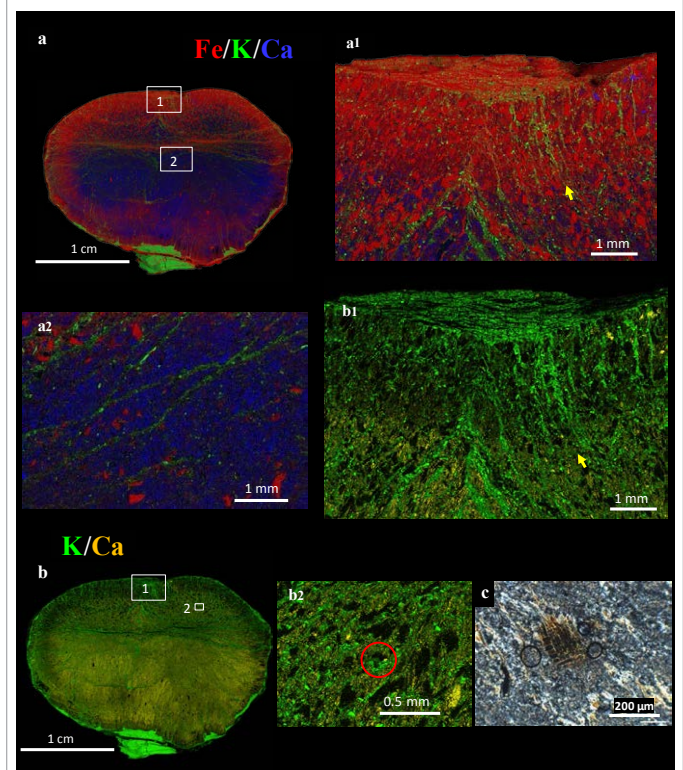


**Figure 11:** Micro-PIXE (Fe -K- Ca) images of a vertical section through an elongated AKOU nodule (AKOU-16); showing the geochemical organization; (A) Distribution of the three elements showing Fe that forms an alteration crown around the nodule, more developed in the upper flattened hemisphere and impregnating the internal median surface and the channels; Ca is distributed more evenly within the nodule; and K most concentrated at the outer limit of the nodule (pelitic sediment), forming a thin film between the nodule and a thin outer Fe 'rim' (for full details see Figure S6); K is dispersed in the mass or concentrated in the channels within the nodule; (A1) Detail of the upper flattened hemisphere where the ferruginous crown shows the flattening of clay channels. Note the high concentration of iron particles. (A2) Criss-crossed clay channels (K) in the Ca-rich central zone of the nodule. (B-B1) Distribution of K and Ca which confirms the distribution of clays around the nodule and the arrangement of these clays parallel to the edge contour, the flattening of clay 'channels' in the iron crown and the crossover alignments of iron particles within clay channels in the nodule; this radial alignment intersects the flattened channels (yellow arrow). (B2) Immediate environment of a small multicellular fossil (red circle); (C) Cell-like hematite clusters showing the surrounding chert matrix and an enclosing matrix of fibrous silicate oriented in the same direction.
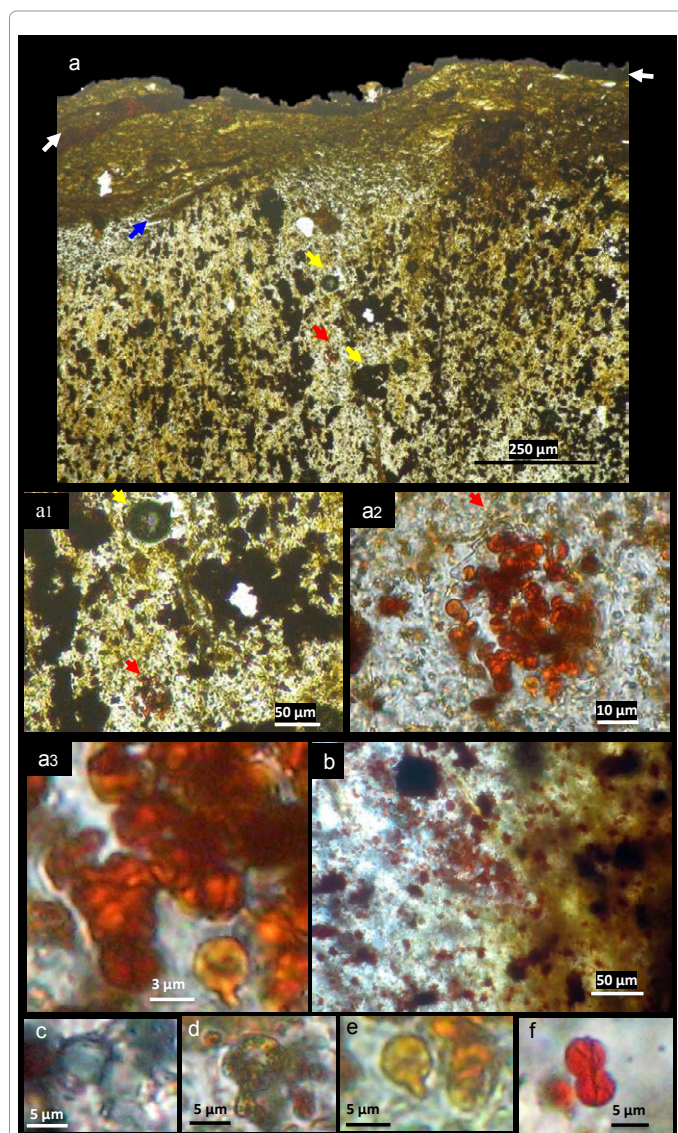
**Figure 12:** Thin section of a nodule's edge zone containing many iron particles generally oriented in alignment with the radial system; (AKOU-1); (A) View of the internal zone with iron particles and the contact with the pelitic sediment, a larger ferruginous filament (more than 250 µm long) into nodule near the edge (blue arrow) intersects radial system; the outer edge of the nodule is surrounded by a thin ferruginous 'rim' (white arrows); three ovoid-shaped particles in an upright position are indicated by the yellow and red arrows; (A1) Close-up of two ovoid forms, one dark coloured and the other rubefied; (A2) Detail of a cluster of cell-like spherulites (50 µm in size) which are surrounded by a translucent thin film; (A3) Detail of the spherulite clusters, some of which have a straight or curved appendix (similar to calcite grains). Flat contact zones can be seen on others that are contiguous; (B) View of an ovoid pocket (top left) with a translucent film containing red spherulites (AKOU-1); (C-F) Various types of spherulites. (C) Grey spherulite with appendix. (D) Spherulites with various colours: grey, green, yellow (AKOU-13). (E) Ferruginized orange-coloured spherulite (OKO-1). (F) Red double spherulite with an internal Y shape (AKOU-20). These spherulites would constitute the remains of the mineralization of biomorphic ovoid particles.

reveal microorganisms and biomorphs that belong to the original organism and that are unrelated to a recent alteration [38].

**Microorganisms:**

a. Silicified and ferruginized filaments are locally preserved in the siliceous mass. They are very dense and intertwined, they are the most abundant microorganisms (Figure 14a). Observed by scanning electron microscopy in the OKO-2 sample, these filaments are very variable in length and range from 1 to 10 µm in diameter. They are both straight and sinuous, and have been fossilized by silica and iron oxides. Using an optical microscope, they are amorphous, straight or irregular and sometimes branched. Some tubular filaments measure 2-3 to 8 µm in diameter and are 50-100 µm long, or more. Their shape is similar to fungal hyphae resulting from post-genetic fungal contamination as the tubes appear to be hollow; however they are syngenetic filaments because they have undergone a process of fossilization by silica. Despite the difficulty in identifying them in thin section, it was possible to identify some elements in the nodule in samples FRA-01-13 and FRA-21 (Figures 14b and S9g).

*b. Cyanobacteria* are among the most abundant microorganisms; they are scattered or found in clusters and are well preserved in the silica-rich nodule. They are easily visible at high magnification in the form of hulls and small filaments measuring 0.5 to 1.5 µm. They are blue-green with often a slightly reddish hue in both parallel and crossed nicols (Figures14c and S9a). Locally the average density can reach 4000-5000 per 100 $\mu m^2$.

**Biomorphs**

a. **Organic carbon:** The organic carbon contents measured on 11 samples nodules vary from 0.10 to 6.86% with 10 samples whose contents are included in 0.10 and 0.18% and 6.86% in one sample (Table S4).

b. Pyritised and altered filaments in the form of hematite-goethite or green filaments are very numerous in the specimens (Figures S9b and S9h-S9i) They measure between 0.5-1 to 3-10 µm in diameter and are often more than 20-50 µm long; they are not directly related to the postgenetic alteration crown. Optic microscopy and Scanning electron microscopy observations highlighted the extremity of a filament with ordered rows of ovoid particles (1-4 microns in size) (Figure 13a) and very fine filaments of 0.4-0.5 µm in diameter formed by a chain of hulls ranging from 0.5-0.6 µm in diameter (Figures 14d). The general physiognomy is that of bacterial or cyanobacterial filaments that were encrusted by iron oxidation.

c. **Spherulites shape:** The spherulites are very numerous; they are most often ferruginized, but some of no ferruginized are grey, green and, yellow-orange or transluside (Figures 12a3, 12c-12f, S5e-S5g, S9d and S9h). They are isolated or very dense, sometimes contained in the 'elongated' pockets with fine translucent silica film (Figures 12a2 and 12b). They are generally aligned, and would be relics of degradation of ovoid biomorphic particles. Each spherulite measures 2-3 to 5-6 µm in diameter. Most are spheroidal, but some are elliptical with external appendix (2 µm), double-spherulite with symmetrical internal Y-shaped forks (Figure 12f). These forms are similar to those of Gunflint chert and are interpreted as the remains of heterotrophic sulphate reducing prokaryotes, preserved during pyritisation [35].

d. **Iron particles:** Nodules contain a multitude of iron particles aligned in the radial system; sometimes in clay channels. Their density varies from one point to another within a same nodule (Figure 11), and from one nodule to another (Figures 10a, 11 and 12). Some multicellular clusters measuring between 50 and 250 µm are preserved among these particles (Figures 11b1, 11b2, 11c and 12). If the radial arrangement of these ferruginous particles predominates, some of them are intersect the radial system (Figures 4d, 12a and 14e).

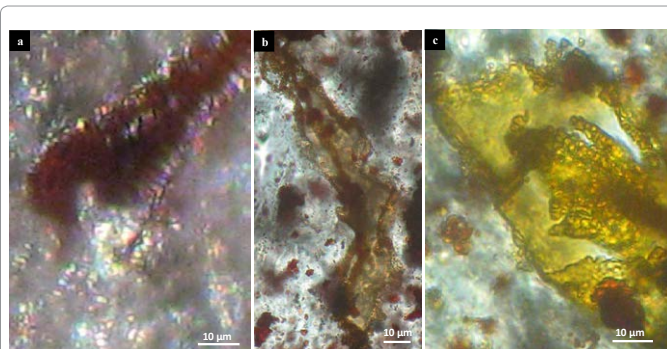e. **Other biomorphs:** Several notable biomorphs were observed.

**Figure 13:** Various other biomorphs in siliceous mass. (A) Extremity of a filament consists of ordered rows (partially degraded) of ovoid particles (cyanobacteria probable, 1- 4 microns in size) in siliceous mass; detached particles are dispersed, and more or less aligned in the mass (crossed nicols, AKOU-2d). (B) Large translucent tubular biomorph with internal filaments, preserved in siliceous mass (crossed nicols, AKOU-3b); (C) Green tubes fragments with granulated "wall", (crossed nicols, OKO-01-45).

In particular, an elongated sheet form, measuring 35-40 μm long and 4-5 μm wide, consisting of a lattice of small orifices ranging from 0.2 to 0.5 μm wide on average resembling algal tissue (Figure 14e). Further scanning electron microscopy examinations made it possible to identify the end of a filament with a ringed structure measuring 1-2 μm in diameter (Figure 14d). Other larger biomorphs are also common

in nodules; they are generally hollow, rubified, translucent tubes with internal filaments, green fragmented tubes with granulated "walls", and vesicles sometimes containing some filaments and spherulites (Figures 13b, 13c, S5h, S9d-S9f and S9i).

**Indices of multicellular microorganisms:** A few pluricellular clusters, some of them large, were identified in two samples. In AKOU-20 (Figure 14g and 14h), we observed a spindle-shaped cell cluster that was 110 μm long. It was formed from a set of around ten elongated hematite shafts ranging from 2 to 5 μm in diameter separated by thin layers of silicate. Each shaft consists of a string of dark grains that are 5-6 μm long and 2 μm wide. At high magnification, very fine, localised transparent tubular filaments that are 0.5 μm in diameter and axially aligned with chains of hematitic cells can be observed. This branched arrangement is reminiscent of an algal procaroyte or eukaryotic organism.

The AKOU-16 sample (Figures 11b2, 11c and 14i-14l) has a remarkable cell cluster measuring 250 μm long caught in the siliceous matter of the nodule's lower right lobe. It is clearly made up of two types of cells: a cortex made up of large cells in a vertical position and an internal "lattice" structure formed by elongated cells in a horizontal position with respect to the others. Larger cells are the cortex cells, which are 15-20 μm wide and 35-40 μm long, have rounded edges and are impregnated with ferric iron (goethite-hematite). The elongated cells are 10 μm wide and 30-40 μm long. They are connected locally by small
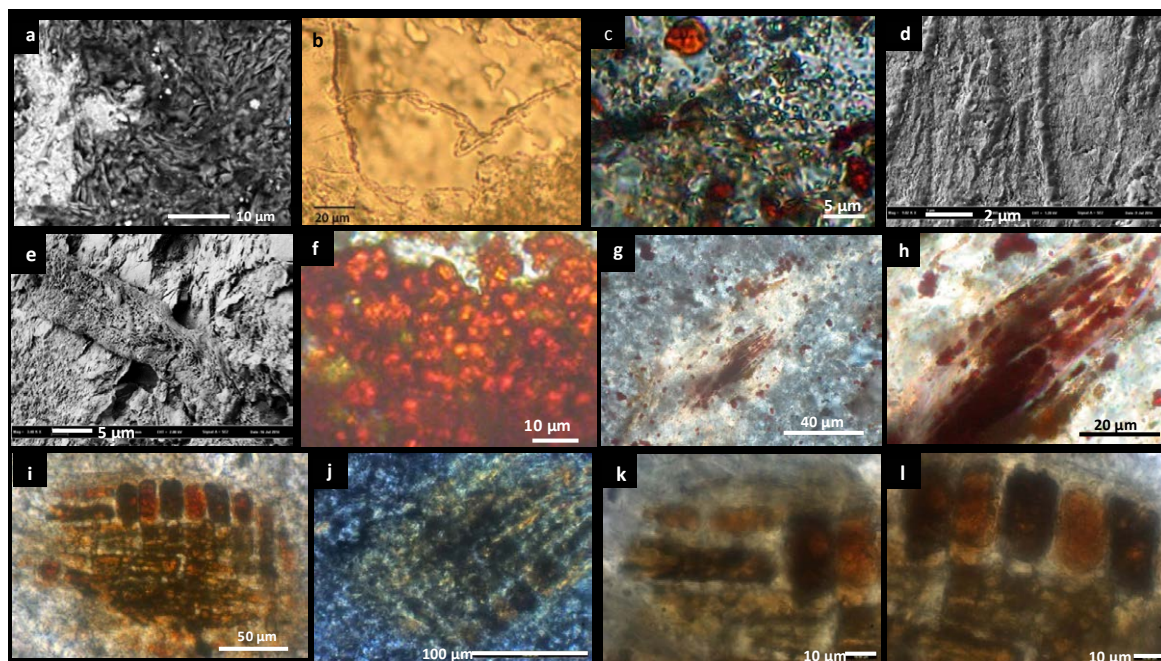


**Figure 14:** Various other types of biomorphs and indices of fossils in the siliceous mass of nodules. (A) Very dense clusters of tangled filamentous microorganisms preserved in the siliceous mass (SEM view, OKO-2); (B) Silicified, branched, translucent and hollow filaments, locally containing a brown inner filament which highlights the translucent wall (parallel nicols, FRA-01-13); (C) Colony of bacteria/ cyanobacteria (crossed nicols, OKO-2). (D) Thin filaments (0.4–0.5 μm in diameter) formed by a chain of hulls of the same size (SEM view, OKO-3); (E) Elongated sheet-like form biomorphs 35-40 μm long and 4-5 μm wide, made up of a weaving of small holes 0.2-0.5 μm wide on average (SEM view, AKOU-17); (F) High density of spherulites of various colours depending on the degree of oxidation. The least numerous green spherulites are little or unferruginised; orange spherulites are slightly ferruginised; red spherulites are most ferruginised. Ferruginisation seems more intence to the surface of the spherulites (parallel nicols, AKOU-14); (G) Cell-like clusters preserved in iron oxide (hematite) (parallel nicols, AKOU 20) showing the cluster lying within the centre of an elongate feature of fibrous silicate and surrounded by silica, plain polarised light, note the main radial direction of the cell-like clusters ; (H) Detail of 'g' showing bundles of elongate filament-like structures separated by clear phyllosilicate (parallel nicols); (I-L) correspond to images of the same multicellular microfossil; (i) Close up view showing the stack of cell-like structures infilled with red iron oxide (hematite), plain polarized light ; (j) View rotated to show more highly pleochroic colours of closely associated fibrous silicate in crossed nicols; (k) Detail of one end showing cluster of elongate cell-like structures, plain polarized light, parallel nicols; (l) Detail of mid portion showing stack of rounded, discoidal cell-like structures, parallel nicols. The cell-like structures are all coated or infilled with iron oxide.

orange filaments 2 μm in diameter and 5-7 μm long. This multicellular organism has a laminated sheath that is visible on the upper edge of the cortex. PIXE high-definition chemical imaging of the microfossil does not show a characteristic mineralogy: there is a siliceous base with the presence of iron. Both the large size of the microfossil (250 x 200 μm) and cells (40-15 μm) suggest an eukaryotic small organism.

## Discussion: Multicellular Consortia in Ductil Nodules

These morphological, micro-morphological, geochemical and isotopic characteristics are arguments in favour of nodules of biological origin. The study of microorganisms and biomorphs supports the hypothesis of consortium-type colonies of symbiotic microorganisms precisely at a time that saw the development of life directly linked with the GOE and photosynthetic activity of cyanobacteria. In addition, the plastic deformation of nodules and sediment indicates the growth of ductile matter near the sediment-waterline in a shallow and calm epibenthic zone. Moreover, relics of multicellular clusters argue in favour of the presence of symbiotic and probable parasitic organisms that have developed in the oxic zone at the sediment-water interface and just below. Fibro-radial and polyphase-type growth are well preserved in a silica-calcite matrix, also highlighted by pyrite and iron oxide. The amorphous calcite framework and their fibro-radial and polyphase appearance is an argument in favour of bacterial or cyanobacterial blooms producing capsular EPS-type calcite, given that these extracellular substances use nucleation for the precipitation of a nanocrystalline proto-calcite of amorphous texture [39].

Nodules with ductile body, complex internal radial fabric oriented from the center to the periphery, internal furrows, linear and flattened clay channels, perpendicular arrangement of biomorphs to the radial system, numerous microorganisms indicate that each nodule likely nucleated around a mass of organic matter already organized, probably linked to photosynthesis on the oxic seafloor (Figure 15a). The organic matter was then quickly buried by thin laminates of pelitic sediment that formed oxidoreducing conditions and provided an abundant source of organic carbon for the sulphate-reduction of bacteria in an anaerobic environment (Figure 15b). This phase is suggested not only by the isotopic composition of the sulphur of the pyritized biomorphs, but also by the numerous spherulites that encrust heterotrophic prokaryotes, including sulphate reducers [35].

The dense preserved pyrite and the filaments that are arranged radially resemble sheathed bacteria oxidising the subsurface sulphur; the latter takes its energy from the oxidation of $H_2S$ produced by sulphate reducers [40]. Some filaments preserved in the iron oxide (hematite), correspond to sheathed iron bacteria [41,42]. Filamentous prokaryotes are known to initiate biofilms which then act as nucleation sites for authigenic mineral growth [43,44].

These morphological, mineralogical and geochemical indicators clearly demonstrate that aerobic-anaerobic consortia are experiencing strong growth on a global scale in shallow sulphuric Paleo-Proterozoic sediments [12]. This confirms the aerobic metabolism of pyritized nodules interpreted as large organisms described in eastern Gabon near Franceville [19,20] and provides valuable details to the understanding of such structures. Communities were seemingly able to flourish not only around hydrothermal vents[11] but much more widely, including silty muds below the sediment-water interface, owing to globally increased levels of seawater oxygenation, bottom water ventilation and sulphate availability [6-9,12].

These aerobic-anaerobic consortia from Akou therefore lived on the seafloor, in a calm, shallow and oxidoreducing environment. Their rapid fossilization was favoured by environmental conditions in the basins and has unfolded in several, almost simultaneous, steps (Figures 15a-15c):
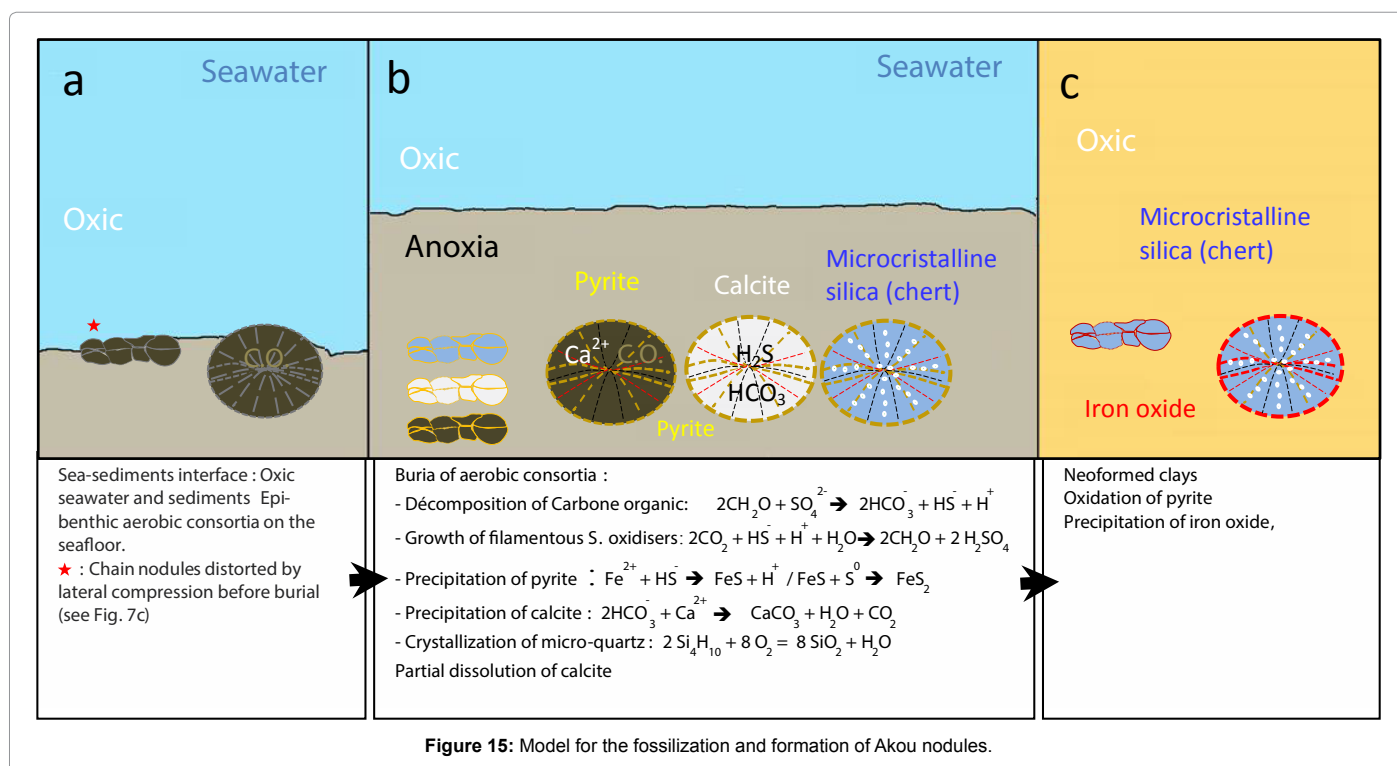
- Burial in an anoxic environment rich in dissolved $SiO_2$;



**Figure 15:** Model for the fossilization and formation of Akou nodules.

| Characteristics | Indicators |
|---|---|
| - Nodule morphology: 2 hemispheres, 1 slice<br>- Complex internal radial fabric (CIR)<br>- Vertical and lateral symmetry<br>- Chains of joined nodules | Complex organization |
| Flexible deformations by lateral compression | Ductility - plasticity |
| Fibro-radial and polyphased internal complexe fabric | Growth |
| Deformed sediments around and between specimens | Growth in soft sediments |
| 13C-depleted carbonaceous matter<br>13C-depleted calcite | Precipitation of calcite by microbial metabolism and degradation of organic matter in anoxic photosynthesis conditions |
| Radiating remnants of biofilms and calcite grains | EPS calcite altered and replaced by silicification |
| Ductile/plastic nodules with CIR containing :<br>- linear and flattened clayey channels<br>- cyanobacteria<br>- many biomorphs (spherulites, filaments, vesicles)<br>- multicellular clusters | Complex nodules hosting:<br>- microbial consortia<br>- probable symbiosis-parasitism by small multicellular eukaryotes |

**Table 1:** Main morphological, mineralogical, isotopic and biogenetic characteristics.

- Enzymatic decomposition and production of $H_2S$, with pyrite crystallization;

- Precipitation of $CaCO_3$ inside specimens;

- Massive precipitation of $SiO_2$ inside specimens, partial dissolution and silicification of amorphous calcite biofilms.

- This was followed by neoformed clays and pyrite alternation into iron oxide.

The complexity and the multiple biogenic characteristics of the Akou nodules (Table 1) now referenced as "*Akouemma*" provide an observable structure that can explain the existence of complex biological consortia of prokaryotic microorganisms, multicellular eukaryotic-type organisms, and larger biomorphs.

During the GOE, biodiversity-friendly conditions therefore enabled the development of large microbial consortia (prokaryotic and multicellular eukaryotic-type organisms) and local symbiosis-parasitism in structured organic matter which have been preserved in a region that has remained stable and was described for the first time in Earth history by ~2.1 Ga.

## Acknowledgements

## References

1. Karhu JA, Holland HD (1996) Carbon isotopes and the rise of atmospheric oxygen. Geology 24: 867-870.

2. Holland HD (2006) The oxygenation of the atmosphere and oceans. Phil Trans R Soc B 361: 903-915.

3. Timothy WL, Reinhard CT, Planavsky NJ (2014) The rise of oxygen in Earth's early ocean and atmosphere. Nature 506: 307-315.

4. Bekker A, Holland HD, Wang PL, Rumble D, Stein HJ, et al. (2004) Dating the rise of atmospheric oxygen. Nature 427: 117-120.

5. Martin AP, Condon DJ, Prave AR, Melezhik VA, Fallick AE, et al. (2013) Dating the termination of the Palaeoproterozoic Lomagundi-Jatuli carbon isotopic event in the North Transfennoscandian Greenstone Belt. Precambr Res 224: 160-168.

6. Kump LR, Junium C, Arthur MA, Brasier A, Fallick A, et al. (2011) Isotopic evidence for massive oxidation of organic matter following the Great Oxidation Event. Science 334: 1694-1696.

7. Schroder S, Bekker A, Beukes NJ, Strauss H, Van Niekerk HS (2008) Rise in seawater sulphate concentration associated with the Paleoproterozoic positive carbon isotope excursion evidence from sulphate evaporites in the ~2.2-2.1 Gyr shallow-marine Lucknow Formation. Terra Nova 20: 108-117.

8. Preat A, Bouton P, Thieblemont D, Prian JP, Ndounze SS, et al. (2011) Paleoproterozoic high delta C-13 dolomites from the Lastoursville and Franceville basins (SE Gabon) Stratigraphic and synsedimentary subsidence implications. Precambr Res 189: 212-228.

9. Brasier AT, Fallick AE, Prave AR, Melezhik VA, Lepland A (2011) Coastal sabkha dolomites and calcitised sulphates preserving the Lomagundi-Jatuli carbon isotope signal. Precambr Res 189: 193-211.

10. Papineau D (2010) Global biogeochemical changes at both end of the Proterozoic insights from phosphorites. Astrobiol 10: 165-181.

11. Lepland A, Joosu L, Kirsimae K, Prave AR, Romashkin AE, et al. (2014) Potential influence of sulphur bacteria on Palaeoproterozoic phosphogenesis. Nature Geosci 7: 20-24.

12. Canfield DE, Ngombi-Pemba L, Hammarlund EU, Bengtson S, Chaussidon M, et al. (2013) Oxygen dynamics in the aftermath of the Great Oxidation of Earth's atmosphere. Proc Nat Acad Sci USA 110: 16736-16741.

13. Planavsky NJ, Asael D, Hofmann A, Reinhard CT, Lalonde SV, et al. (2014) Evidence for oxygenic photosynthesis half a billion years before the Great Oxidation Event. Nature Geosci 7: 283-286.

14. Kopp RE, Kirschvink JL, Hilburn IA, Nash CZ (2005) The Paleoproterozoic snowball Earth A climate disaster triggered by the evolution of oxygenic photosynthesis. Proc Nat Acad Sci USA 102: 11131-11136.

15. Catling DC, Claire MW (2005) How Earth's atmosphere evolved to an oxic state A status report. Earth Plan Sci Lett 237: 1-20.

16. Han TM, Runnegar B (1992) Megascopic eukaryotic algae from the 2.1-billion-year-old Negaunee iron-formation Michigan. Science 257: 232-235.

17. Amard B, Bertrand-Sarfati J (1997) Microfossils in 2000 Ma old cherty stromatolites of the Franceville Group Gabon. Precambr Res 81: 197-221.

18. Tomitani A, Knoll AH, Cavanaugh CM, Ohno T (2006) The evolutionary diversification of cyanobacteria Molecular-phylogenetic and paleontological perspectives. Proc Nat Acad Sci USA 103: 5442-5447.

19. El Albani A, Bengtson S, Canfield DE, Bekker A, Macchiarelli R, et al. (2010) Large colonial organisms with coordinated growth in oxygenated environments 2.1 Gyr ago. Nature 466: 100-104.

20. El Albani A, Bengtson S, Canfield DE, Riboulleau A, Rollion Bard C, et al. (2014) The 2.1 Ga Old Francevillian Biota: Biogenicity, Taphonomy, Biodiversity. PLoS ONE 9.

21. Feys R, Greber C, Pascal M (1966) About the age of the continental flora discovery of coal and phytomorphic in Francevillien ( Precambrian Gabon ) . Bull Soc Geol France, 7th Series, vol. VIII: 638-641.

22. Dutkiewicz A, George SC, Mossman DJ, Ridley J, Volk H (2007) Oil and its

biomarkers associated with the Palaeoproterozoic Oklo natural fission reactor Gabon. Chem Geol 244: 130-154.

23. Pambo F, Guiraud M, Quesne D, Gauthier-Lafaye F, Azzibrouck G, et al. (2006) The Proterozoic Franceville Basin (SE Gabon) an example of interaction between marine sedimentation and extensional faulting. Africa Geosci Rev 13: 77-106.

24. Gauthier-Lafaye F, Weber F (2003) Natural nuclear fission reactors time constraints for occurrence, and their relation to uranium and managanese deposits and to the evolution of the atmosphere. Precamb Res 120: 81-100.

25. Moussavou M, Edou Minko A (2006) Contribution the thermo- tectonic history of the Precambrian N'goutou ring complex by geochemistry and geochronology U/Pb accessory minerals (Francevillien Okondja Basin, Gabon). Africa Geosci Rev 13: 53-61.

26. Bros R, Stille P, Gauthier-Lafaye F, Weber F, Clauer N (1992) Sm-Nd isotopic dating of Proterozoic clay material. An example from the Francevillian sedimentary series. Earth Plan Sci Lett 113: 207-218.

27. Horie K, Hidaka H, Gauthier-Lafaye F (2005) U-Pb geochronology and geochemistry of zircon from the Franceville series at Bidoudouma, Gabon, Geochim, Cosmochim. Acta 69: A11.

28. Bouton P, Thieblemont D, Gouin J, Cocherie A, Guerrot C, et al. (2009) Explanatory notes for the Geological Map of the Republic of Gabon to 1/200 000, Franceville- Boumango sheet. Editions MCB - Ministry of Mines, Oil, Hydrocarbons p. 79.

29. Konhauser K, Riding R (2012) Bacterial biomineralization. In: Knoll AH, Canfield DE, Konhauser KO (eds.), Fundamentals of Geobiology. John Wiley & Sons, Chichester, UK, pp. 105-130.

30. Couradeau E, Benzerara K, Gerard E, Moreira D, Bernard S, et al. (2012) An early-branching microbialite cyanobacterium forms intracellular carbonates. Science 336: 459-462.

31. Kamennaya NA, Ajo-Franklin CM, Northen T, Jansson C (2012) Cyanobacteria as Biocatalysts for Carbonate Mineralization. Minerals 2: 338-364.

32. Weber F, Gauthier-Lafaye F (2013) No proof from carbon isotopes in the Francevillian (Gabon) and Onega (Fennoscandian shield) basins of a global oxidation event at 1980-2090 Ma following the Great Oxidation Event (GOE) CR Geosci 345: 28-35.

33. Reid RP, Visscher PT, Decho AW, Stolz JF, Bebout BM, et al. (2000) The role of microbes in accretion, lamination and early lithification of modern marine stromatolites. Nature 406: 989-992.

34. Baumgartner LK, Spear JR, Buckley Daniel H, Pace NRR, Reid P, et al. (2009) Microbial diversity in modern marine stromatolites, Highborne Cay, Bahamase. Environmental Microbiology 11: 2710-2719.

35. Wacey D, McLoughlin N, Kilburn MR, Saunders M, Cliff JB, et al. (2013) Nano-scale analysis of pyritized microfossils reveals differential heterotrophic consumption in the ~1.9 Ga Gunflint Chert. Proc Nat Acad Sci 110: 8020-8024.

36. Kasting JF, Tazewell Howard M, Wallmann K, Veizer J, Shields G, et al. (2006) Paleoclimates, ocean depth, and the oxygen isotopic composition of seawater. Earth Plan Sc Lett 252: 82-93.

37. Knoll AH, Barghoorn ES (1976) A gunflint-type microbiota from the Duck Creek dolomite, western Australia. Orig Life 7: 417-423.

38. Skinner HCW, Fitzpatrick RW (1992) Biomineralization processes of iron and manganese, modern and ancient environments. Catena Supplements 21: 433.

39. Dittrich M, Kurz P, Wehrli B (2004) The role of autotrophic picocyanobacteria in calcite precipitation in an oligotrophic lake. Geomicrobiology Journal 21: 45-53.

40. Hogslund S, Revsbech NP, Kuenen JG, Jorgensen BB, Gallardo VA, et al. (2009) Physiology and behaviour of marine Thioploca. ISME Journal 3: 647-657.

41. Planavsky N, Rouxel O, Bekker A, Shapiro R, Fralick P, et al. (2009) Iron oxidising microbial ecosystems trhived in the late Proterozoic redox stratified oceans. Earth Plan Sci Lett 286: 230-242.

42. Schieber J, Glamoclija M (2007) Microbial mats built by iron bacteria, a modern example from southern Indiana. In: Schieber J (ed.), Atlas of microbial mat features preserved within the clastic rock record Elsevier pp. 233-244.

43. Costerson JW (2007) The Biofilm Primer. Springer, Berlin, pp. 199.

44. Brasier AT, Andrews JE, Kendall AC (2011) Diagenesis or dire genesis? The origin of columnar spar in tufa stromatolites of central Greece and the role of chironomid larvae. Sedimentol 58: 1283-1302.